

# Control of Stress Propagation in the Cytoplasm by Prestress and Loading Frequency

Shaohua Hu\* and Ning Wang†

**Abstract:** One fundamental question in cell biology is how mechanical stresses are distributed inside the cytoplasm. Recently we have developed a synchronous detection approach to map cytoplasmic displacements and stresses using yellow fluorescent protein tagged mitochondria as fiducial markers of the cytoskeleton (CSK) in response to a localized load applied via an RGD-coated magnetic bead (7). We have shown that stresses are propagated to remote sites in the cytoplasm, a finding that contradicts continuum model predictions. Here we show that long distance force propagation in the cytoplasm was abolished when the contractile prestress in the CSK was lowered by relaxing agents and enhanced when the prestress was increased by contractile agonists. Surprisingly, when the loading frequency was varied from 0.03 Hz to 30 Hz, the total area of induced displacements (an index of the extent of stress propagation) first increased with loading frequency and then decreased with loading frequency. These results demonstrate that the long distance force propagation in living adherent cells might be controlled by the level of contractile prestress in the CSK and by the loading frequency.

## 1 Introduction

One fundamental question in mechanotransduction is how stresses are propagated and distributed inside the cytoplasm. Established evidence demonstrates that integrins and focal adhesions are the major initial pathways of force transmission between an adherent cell and the extracellular matrix (1-5); furthermore, the cytoskeleton (CSK) is known to be the primary stress-bearing elements inside the cytoplasm (6). However, it is still not clear how a localized load at the cell surface propagates along the CSK lattice. Recently, using a sensitive method of synchronous detection to quantify load-

induced displacements, we have demonstrated that a localized load applied via the integrin receptors through a RGD-coated 4.5- $\mu$ m magnetic bead, leads to concentrated strains/stresses at cytoplasmic and intra-nuclear sites *remote* from the site of the applied load (7-9). This is a surprising finding since it departs significantly from predictions of conventional continuum mechanics-based cell models (10) that predict that the stress will dissipate inversely with the square of the distance from the site of applied load. Furthermore, we found that disrupting filamentous actin with cytochalasin D or inhibiting the pre-existing tension in the CSK (prestress) in the cell by overexpressing caldesmon abolished this long distance force propagation (7), suggesting that the prestress plays a major role in mediating the “action at a distance” phenomenon. In order to further explore the role of the prestress, in this study, we altered the prestress using a number of different pharmacological agents. *In vivo*, cells experience mechanical loads of different frequencies. For example, human airway smooth muscle cells in the lung experience breathing-induced mechanical stretching at  $\sim$ 0.2 Hz and heartbeat-induced loading at  $\sim$ 1.0 Hz. We hypothesized that loading frequency would influence the extent of stress propagation similar to its effects on cell stiffness if cell stiffness was a major determinant of stress propagation. Here we examined the effects of loading frequency on stress propagation.

## 2 Methods

**Cell Culture.** Human airway smooth muscle cells were isolated from tracheal muscle of lung transplant donors and cultured using a previously published method (11). Adenovirus vectors were used to transiently infect the cell with YFP-cytochrome C oxidase, an enzyme located exclusively at the inner membrane of the mitochondria. The detailed protocols were described previously (7). The cells were plated sparsely on type-1 collagen-coated dishes in serum free medium overnight before experiments. Since whether stress propagation is related to cell

\*Physiology Program, Harvard School of Public Health, Boston, MA 02115

†Corresponding author, Department of Mechanical and Industrial Engineering, University of Illinois at Urbana-Champaign, Urbana, IL 61801. Email: nwangrw@uiuc.edu

cycle progression was not the focus of this project, we limited our study to interphase cells by serum depriving them.

**Load application and synchronous detection of induced displacements.** We applied mechanical torques via a magnetic bead to an adherent cell in a dish under a microscope at 37°C. Previously we showed that magnetic beads coated with acetylated low density lipoproteins (AcLDL) that bind specifically with nonadhesion molecule scavenger receptors resulted in only localized CSK deformation in the vicinity of the bead (4). Therefore in this study we focused on probing the CSK via the integrin receptors. Ferromagnetic beads (4.5- $\mu\text{m}$  diameter or 0.8- $\mu\text{m}$  diameter) coated with Arg-Gly-Asp (RGD)-containing peptides, specific ligands for integrin receptors, were bound to the apical surface of the adherent cells for 15 min (or 5 min for a 0.8- $\mu\text{m}$  bead). The beads were magnetized using a strong (1,000 G) and short (<0.1 ms) magnetic field pulse oriented at the horizontal direction. A sinusoidally varying vertical magnetic “twisting” field was applied at 0.03125, 0.3125, 0.83, 5, 15, or 30 Hz. The fluorescent image exposure time was 300, 200, 100, 10, 5, 5 ms respectively. The maximum rate of image data acquisition is not only limited by the CCD camera speed, but also by the data storage speed of the computer. For example, it requires 120 ms to capture and store each 600 pixel by 600 pixel image into our computer. To prevent data jamming and image storage loss, time delay between any two images should be at least 120 ms. To achieve this, an image acquisition heterodyning strategy was used for loading frequencies higher than 0.83 Hz (one cycle = 1.2048 sec; an 11-image acquisition at 120 ms per image takes 1.2 sec, slightly less than the cycle) to take advantage of the periodicity of the cyclic loading, an approach to decrease the image acquisition rate. For example, for the 5 Hz case, after the 1<sup>st</sup> fluorescent image was taken at the beginning of the 1<sup>st</sup> cycle, the second fluorescent image was only taken at a time that was precisely 1/10 of a cycle after the start of the 2<sup>nd</sup> cycle (i.e., 220 ms after the 1<sup>st</sup> image). Therefore it took 2.2 sec (11 cycles) to complete an 11-image acquisition at 5 Hz loading frequency. For the 30 Hz case, the 2<sup>nd</sup> image was taken at the time that was 1/10 of a cycle from the start of 5<sup>th</sup> cycle (i.e., 136.7 ms after the 1<sup>st</sup> image). It took 1.367 sec (41 cycles) to complete an 11-image acquisition. The resulting bead translational displacements caused by bead rotation were

determined by quantifying the bead center movement using an intensity-weighted-center-of-mass algorithm. The bead lateral movement was used to calculate the corresponding dynamic modulus using the established method (12). Fluorescent image acquisition was phase-locked to the twisting field such that 10 images are taken during one twisting cycle. Using a cross-correlation approach, we computed the induced displacement field by comparing corresponding arrays between two images taken at different phases during the twisting cycle. We shifted the arrays of the second image by sub-pixel increments (1/25 of a pixel) in the Fourier-domain until the mean square differences of the pixel-intensities between the shifted array and the corresponding array from the first image reached a minimum. The resolution of the displacement measurements was  $\sim 5$  nm. Intracellular traction fields (i.e., an index of the stress field) at a focal plane were computed from displacement fields, using the magnetic bead displacement to estimate the cell shear modulus (7).

### 3 Results

#### 3.1 The synchronous detection approach resolves load-induced displacements to a few nanometers

Recently we reported the method of the synchronous detection (7). This approach is simple and straightforward. Here we describe it in some details. After a single, 4.5- $\mu\text{m}$  magnetic bead coated with integrin ligands was bound to the cell surface for  $\sim 15$  min (Fig. 1A) on an adherent cell infected with adenovirus YFP-mitochondria (Fig. 1B). The bead was magnetized in the horizontal direction and then rotated by a sinusoidal twisting magnetic field applied along the vertical direction. The magnetic field was applied at a fixed frequency of 0.3 Hz. Fluorescent images of the cell were collected at the rate of 10 images per twisting cycle and the induced displacements of the mitochondria that were synchronized with the input magnetic fields were quantified using a cross-correlation approach. The mitochondrial displacement exhibited a phase delay relative to the input signal, indicative of viscoelastic behaviors (Fig. 1C). By mapping the signal to noise (S/N) ratio for the entire field of view (Fig. 1D) and only keeping the induced displacements whose S/N ratio was higher than 3, we obtained the induced displacement map of this cell (Fig. 2A). There was a large spot of concentrated displacements  $\sim 20$   $\mu\text{m}$  away from the bead (Fig. 2A), consistent with our previous report (7). Using

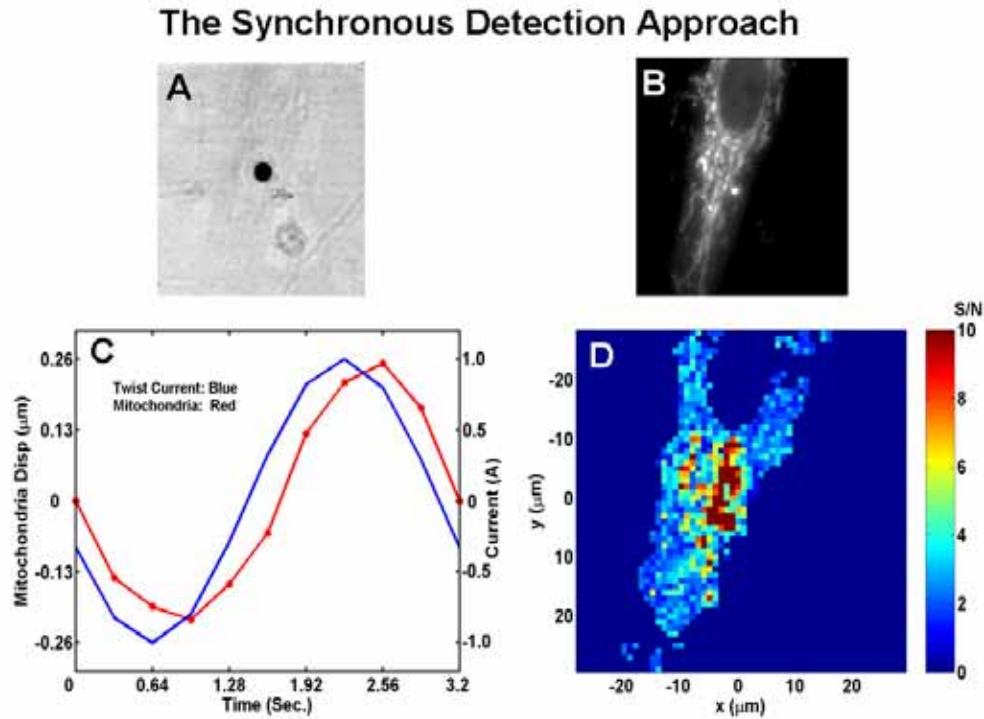


**Figure 1** : The synchronous detection method. A: a  $4.5\text{-}\mu\text{m}$  ferromagnetic bead (the black dot in the center) is bound to the apical surface of an adherent airway smooth muscle cell. B: the fluorescent image of the cell infected with adenovirus YFP-mitochondria. C: the input twisting current (blue line) and the displacements of a mitochondrion (red dots) as a function of one twisting cycle. D: the map of the measured signal to noise ratio (S/N) at the peak displacement.

the magnetic bead displacement on the cell surface to estimate the average cell elastic modulus, we computed an intracellular traction map at this x-y focal plane that corresponded to the displacement field (Fig. 2D). Because the true local stiffness at different sites was not known, this apparent “stress” map was only a crude approximation of the actual local stress distribution at this x-y plane. Using a  $0.8\text{-}\mu\text{m}$  diameter RGD-coated bead to apply the local load, we also observed the long distance force propagation in the cytoplasm (Appendix, Fig. 7), suggesting that the “action at a distance” phenomenon is not an artifact caused by the large apical focal adhesion that was recruited to the  $4.5\text{-}\mu\text{m}$  bead.

### 3.2 Contractile prestress controls long distance force propagation

Recently we have demonstrated that adherent human airway smooth muscle cells exhibit significant level of

prestress under resting conditions (11, 13). We have also shown that lowering the prestress by overexpressing caldesmon in the cell or disrupting the actin CSK with cytochalasin D completely abolished the long distance force propagation phenomenon (7). To further examine the role of prestress in force propagation, we modulated the contractile prestress with known pharmacological agents. Increasing the prestress with contractile agonist histamine ( $10\ \mu\text{M}$ ) led to time-dependent changes in the number and patterns of focused displacements and stresses in the CSK (Fig. 2); there were dramatic alterations in the displacement and stress patterns 10 s after histamine treatment (Fig. 2B, 2E). After 1 min of histamine treatment, the displacements and stresses exhibited different patterns from the patterns after 10 s histamine (Fig. 2C, 2F). In contrast, decreasing the prestress with bronchodilator isopreterenol (Iso) ( $1\ \mu\text{M}$ ), led to a time-dependent decrease in the number of focused displacements at remote sites; 2 min after Iso, there were

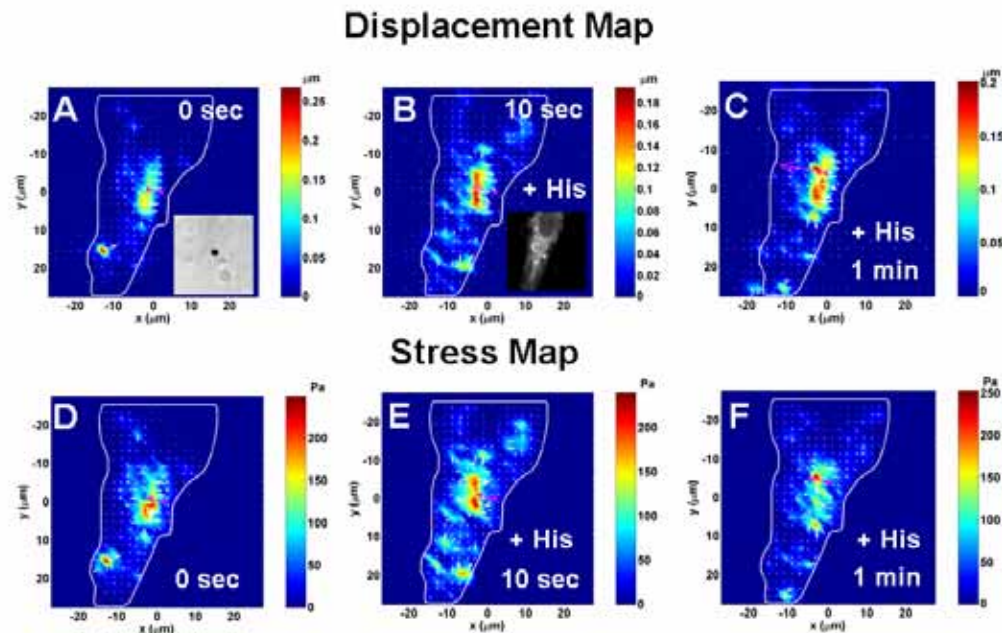


**Figure 2** : Elevation of contractile prestress in the CSK alters patterns of displacements/stresses. A and D: displacement (A) and stress (D) maps of the cell at baseline conditions. B and E: displacement (B) and stress (E) maps of the same cell 10 sec after contractile agonist histamine (His) treatment ( $1 \mu\text{M}$ ). C and F: displacement (C) and stress (F) maps of the same cell 1 min after histamine treatment. Color represents the magnitudes and white arrows represent the directions of the displacements or stresses. Pink arrow represents the position of the magnetic bead and the direction of bead center lateral movement. Other cells showed similar patterns.

no dramatic changes relative to the controls (Fig. 3B, 3E); 4 min after the drug treatment, there were almost no concentrated displacements or stresses outside the vicinity of the bead (Fig. 3C, 3F). Taken together, these results suggest that the prestress plays a key role in mediating the force propagation along the CSK. As a control, we continuously twisted an RGD-coated bead for 30 s and mapped the displacements of YFP-mitochondria as a function of time. No visible changes were detected in the displacement maps (**Appendix**: compare Fig. 8 lower left image with lower right image) or in the fluorescent images (Fig. 8 upper images), suggesting that the dramatic changes observed in the displacement maps or the stress maps in Figs. 2 and 3 were the results of the prestress-modulating drugs.

### 3.3 Stress propagation varies with loading frequency

Recently, it has been shown in several types of adherent cells that the stiffness of the cell increases as a power-law with the loading frequency (12). Because mitochondria are physically connected with microtubule filament systems via motor protein kinesin and dynein (14), the displacements of mitochondria are indexes of the displacements or deformation of the microtubule networks. Since the cell stiffness increases with loading frequency; in other words, the magnetic bead displacement decreases with loading frequency for a given load, we hypothesized that, if the cell stiffness was a major determinant of stress propagation in the CSK, the displacements of YFP-mitochondria should decrease with loading frequency in a similar manner. To test this hypothesis, we quantified the peak displacements of the mitochondria in response to loading frequencies varying from 0.03 to 30 Hz.

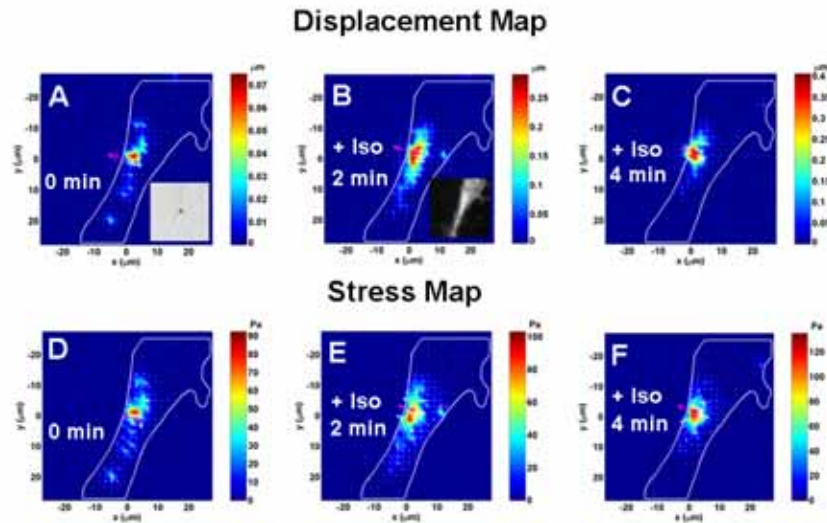


**Figure 3** : Inhibition of contractile prestress in the CSK decreases the extent of stress propagation. A and D: displacement (A) and stress (D) maps of the cell at baseline conditions. B and E: displacement (B) and stress (E) maps of the same cell 2 min after relaxing agent isoproterenol (Iso) treatment ( $1 \mu\text{M}$ ). C and F: displacement (C) and stress (F) maps of the same cell 4 min after Iso treatment. Color represents the magnitudes and white arrows represent the directions of the displacements or stresses. Pink arrow represents the position of the magnetic bead and the direction of bead center lateral movement. Other cells showed similar results.

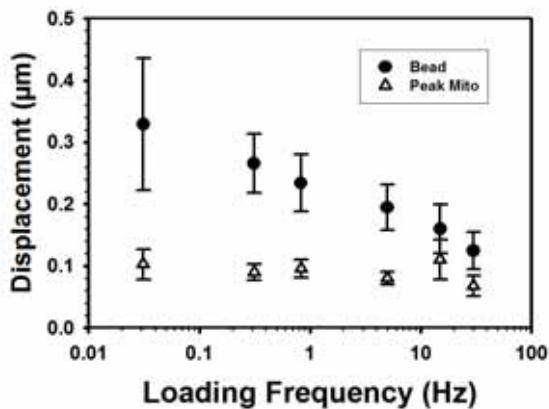


**Figure 4** : The peak displacements of the mitochondria (open triangles) and the lateral displacements of the magnetic bead center (closed circles) as a function of loading frequency. It is clear that bead displacements decrease much more rapidly with frequency than peak mitochondrial displacements.  $N = 8$  cells at 0.03 Hz, 24 cells at 0.3, 0.83, and 5 Hz, and 13 cells at 15 and 30 Hz.

As expected, the magnetic bead displacement ( $D_{\text{bead}}$ ) decreased with the loading frequency ( $f$ ) (Fig. 4, circles). On the log-log scale this dependence was linear, indicating a power law behavior. A linear regression line fit in a log-log plot shows that  $\log D_{\text{bead}} = -0.655 - 0.133 \log f$ . Hence the power-law exponent of frequency is  $-0.133$ . Since the magnetic bead displacement is inversely proportional to the cell stiffness for a given applied torque, these data are consistent with the published data of increasing power-law dependence of stiffness (exponent  $\sim 0.2$ ) with loading frequency (12).

Interestingly, the peak magnitudes of the YFP-mitochondria displacement ( $D_{\text{mito}}$ ) decreased only slightly in response to loading frequency (Fig. 4, triangles). A linear regression line fit in a log-log plot shows that  $\log D_{\text{mito}} = -1.041 - 0.032 \log f$ . The exponent of frequency is  $-0.032$ . Since mitochondria displacements are fiducial markers of microtubule displacements and deformation, these data suggest that the peak microtubule displacements and deformation are much less sensitive to loading frequency than the shear stiffness is.

To examine the effect of loading frequency on stress

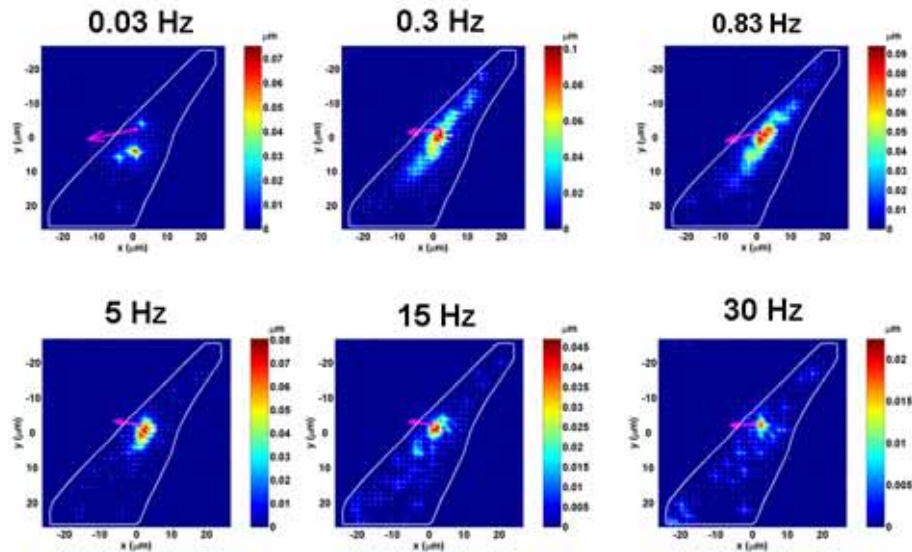


**Figure 5 :** The effect of loading frequency on force propagation areas in a representative cell (the same cell as in Appendix Fig. 9). It appears that the total area of displacements increased first with loading frequency and then decreased with frequency, although there were still apparent displacements at distances  $> 20 \mu\text{m}^2$  at 30 Hz. Note that the displacement scales are different at different frequencies. Color represents the magnitudes and white arrows represent the directions of the displacements. Pink arrow represents the position of the magnetic bead and the direction of bead center lateral movement.

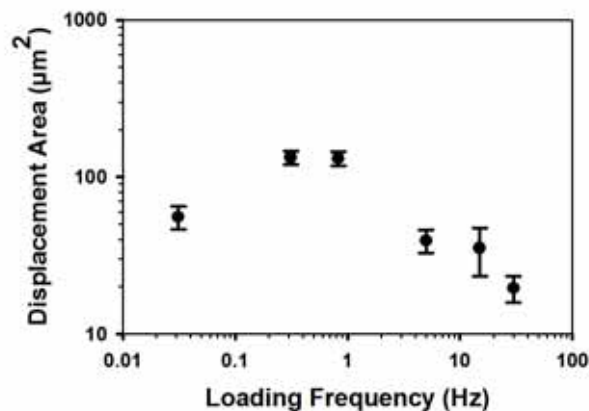


**Figure 6 :** The total area of load-induced displacements as a function of loading frequency. It appears that the displacement area increased first and then decreased with loading frequency. The loading frequency was varied randomly.  $N = 8$  cells at 0.03 Hz, 24 cells at 0.3, 0.83, and 5 Hz, and 13 cells at 15 and 30 Hz.

propagation, we varied the loading frequency from 0.03 to 30 Hz and quantified the total area of induced displacements, i.e., sum of all the pixel areas of the induced mitochondria displacements that have an  $S/N > 3$ . This total area is the area of the mitochondria that has been displaced by the magnetic bead and reflects how extensive the stress propagates in the cytoplasm: the greater the area, the more extensive the stress propagates. Fig. 9 shows the cell/bead images and fluorescent images of a representative cell. There were no visible changes in fluorescent images or bead images at different frequencies. However, surprisingly, as the loading frequency increased from 0.03 Hz to 30 Hz, the total area of the induced displacements, first increased at 0.3 Hz to  $117 \mu\text{m}^2$ , did not change much at 0.8 Hz, and then decreased monotonously from 0.8 to 30 Hz (Fig. 5). The summarized data are shown in Fig. 6.

## 4 Discussion

The major findings of this study are that long distance force propagation in the cytoplasm is modulated by the contractile prestress of the CSK and by the loading frequency.

By what mechanisms do living cells transmit and transduce surface mechanical forces is a central question in cell mechanics. Although different models have been proposed, the underlying mechanism of mechanotransduction still remains unclear. The proposed cell mechanotransduction models can be classified into two categories: *Indirect*: ATP concentration model (15); inter-cell spacing/EGF concentration model (16); *Direct*: non-specific membrane deformation model (17, 18); adhesion molecule/CSK model (3, 5, 19-22). In the adhesion molecule/CSK model, the current focus is on the activation of focal complexes at the force application site and the subsequent diffusion or translocation of signaling molecules from the site of force application into the deep cytoplasm or the nucleus. This idea is built on the assumption that a local force only leads to a local deformation, a well-known behavior of conventional engineering materials, and is consistent with continuum model predictions. Our recent experimental evidence in living adherent cells, demonstrates, however, that a local force can be propagated to remote sites, far away from the loading site (7-9), representing dramatic departures from these conventional model predictions. Importantly, we have shown that disrupting the actin CSK, reducing the prestress by over-expressing caldesmon, or inhibiting actin bundle formation by plating the cells on nonspecific substrate such as poly-L-lysine, all led to abolishment of the “action at a distance” phenomenon (7).

In this study, we have further shown that when the contractile prestress in the CSK is modulated with specific contractile agonists or relaxing agents, the patterns of stress-induced displacements and stresses are altered dramatically. When the prestress is lowered by the relaxing agent isopreterenol, the “action at a distance” phenomenon disappears and the cell behaved just like a conventional engineering material. In contrast, when the prestress is elevated with contractile agonist histamine, the number of concentrated displacements/strains increases. These results strengthen the previous findings and are consistent with the notion that CSK contractile prestress plays a major role in mediating the “action at

a distance” behavior. These data are consistent with our previous findings that tensed actin bundles play a key role in mediating the long distance force propagation (7, 9).

By what mechanism does the prestress modulate the distribution of the displacements in the CSK? Recently we have proposed a tensed actin bundle model to explain the “action at a distance” behavior (23). This model is built on the idea that a tensed actin bundle or a prestressed stress fiber has a modulus that is much higher than the modulus of the surrounding CSK matrix such that a force propagating along the tensed bundle does not decay as rapidly in space as homogeneous materials do. The length scale of force propagation is proportional to square root of ratio of the actin bundle modulus to the CSK matrix modulus. This model is supported by recent experimental data from Sato’s group who have demonstrated that the modulus of a single stress fiber is  $\sim 1$  MPa (24) whereas the modulus of the CSK matrix is only  $\sim 1$  KPa. From these data, the length scale of force propagation is estimated to be  $\sim 70$   $\mu\text{m}$  in living adherent cells that have actin bundles (23). If our model is valid, our current data suggest that these prestress-modulating drugs may preferentially increase/decrease the tension in the actin bundles/stress fibers much more than they modulate the tension in the rest of the CSK matrix (23). The reason is that if histamine (or isopreterenol) increase (or decrease) the tension in the actin bundles/stress fibers in the same proportion as it does to the CSK matrix tension, then there will be no preferential stiffening of the actin bundle/stress fiber relative to the CSK matrix, and thus no modulation of the extent of force propagation. Future experiments are needed to test this preferential stiffening idea directly. Since these prestress-modulating drugs alter the crosslinking of myosin and actin, we cannot rule out the possibility that the long distance force propagation is also partially facilitated by crosslinking of myosin and actin. However, the increase in the number of focused displacements/strains after histamine treatment appears to be much less than the presumed increase in the number of crosslinked myosins and actins based on the increase magnitudes in the contractile forces (11), suggesting that the crosslinking of myosin and actin may be necessary but not sufficient for long distance force propagation.

Fabry et al. (12) demonstrated a few years ago that stiffness of living adherent cells exhibits weak “power law” (power exponent  $\sim 0.2$ ) dependence on loading fre-

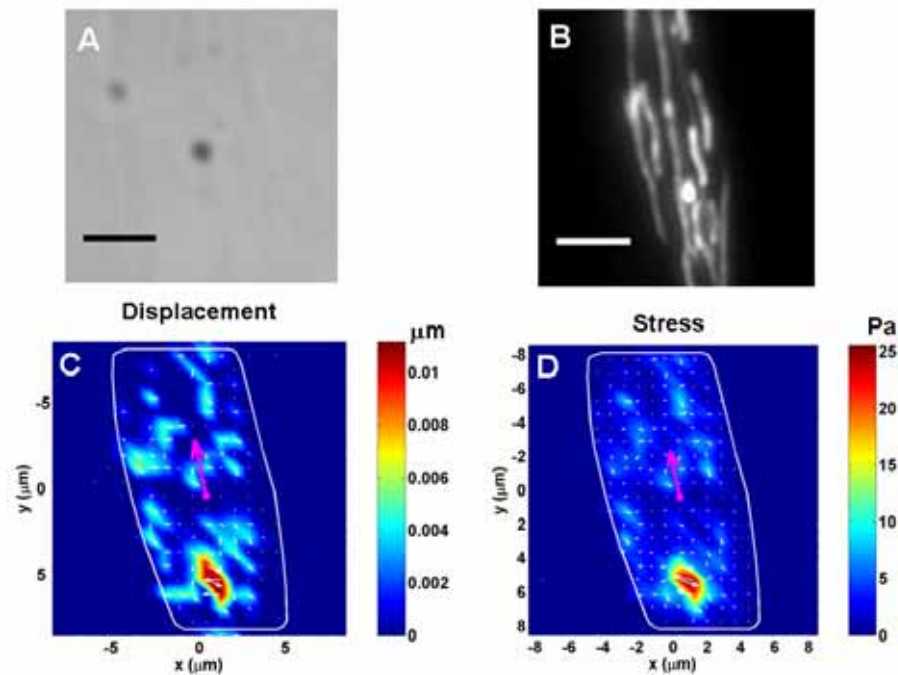


**Figure 7** : A 0.8- $\mu\text{m}$  diameter RGD-coated magnetic bead induced focused displacements at sites remote from the bead. A: the bright field image of the cell with the bead in the center. B: the fluorescent image of the same cell. C: the load-induced displacement map. D: the computed 2D apparent stress map. Note that there was a large concentration of displacements/stresses  $\sim 6\mu\text{m}$  away from the bead, whereas nearby mitochondria were not displaced, suggesting specific stress propagation pathway in the cytoplasm of the cell. Color represents the magnitudes and white arrows represent the directions of the displacements. Pink arrow represents the position of the magnetic bead and the direction of bead center lateral movement. Other cells showed similar patterns. Scale bars = 5  $\mu\text{m}$ .

quency and they likened this behavior to that of a soft glass. Stamenovic et al. (25) have described an empirical relationship between the prestress and the exponent of the power law. We speculated that stress propagation in the CSK would be dependent on loading frequency in a similar manner if the stiffness of the cell is a major determinant of force propagation. However, we have found that, for a given prestress, the peak mitochondria displacements (an index of peak microtubule displacements/deformation) decrease much more slowly with loading frequency for a fixed applied stress than the bead displacements do. This is consistent with previous findings that microtubules contribute only a small fraction to the prestress and stiffness of the cell in highly spread cells (13). The bead displacement is a measure of cell stiffness that includes contributions from cell membrane, focal adhesion proteins, F-actin network, and other CSK (microtubules and intermediate filaments) networks. At the loading frequency of 30 Hz, the magni-

tudes of the bead displacements approach those of peak mitochondria displacements (Fig. 4), suggesting that the membrane/focal adhesion/actin network complex might be the primary structures responsible for the stiffness-frequency response at frequencies from 0.03 to 30 Hz.

Surprisingly, when the applied loading frequency is varied from 0.03 Hz to 30 Hz, the total induced displacement area, which is an index of the extent of stress propagation in the cytoplasm, did not exhibit a monotonic decrease with frequency as the bead displacements do. Rather, the total displacement area increased first from  $\sim 60\mu\text{m}^2$  at 0.03 Hz to  $\sim 120\mu\text{m}^2$  at 0.3 Hz and then decreased with frequency to a value of  $\sim 18\mu\text{m}^2$  at 30 Hz (Fig. 6). On the other hand, the finite element analysis (7, 10) of a homogeneous elastic material predicts that the total (comparable) displacement area would be  $\sim 10\mu\text{m}^2$ , assuming 10% bead area was embedded. Therefore, as the loading frequency increases, the induced displacement area appears to approach that of

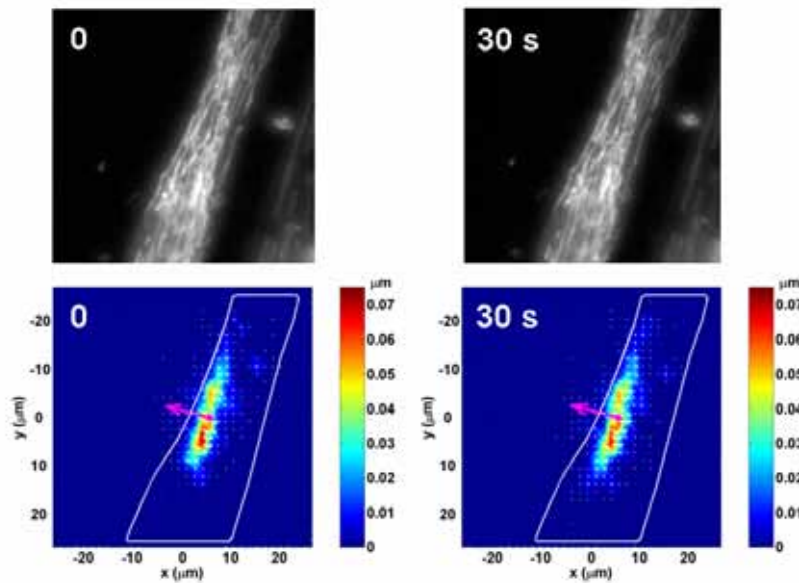


**Figure 8** : A control cell at baseline conditions exhibits little changes in fluorescent images or displacement images. Left images: the fluorescent image (top left) and the displacement map (lower left) of the cell at time 0. Right images: the fluorescent image (top right) and the displacement map (lower right) of the cell 30 sec after a local load applied at 0.3 Hz and 50 Gauss. Color represents the magnitudes and white arrows represent the directions of the displacements. Pink arrow represents the position of the magnetic bead and the direction of bead center lateral movement.

continuum model predictions. However, since mitochondria displacements are only fiducial markers of the CSK displacements/deformation, displacements of some CSK structures were likely not measured. Thus these mitochondria displacement areas could be a significant underestimate of the true areas of the CSK that were deformed. Nevertheless, our conclusion on the relative change of the displacement area in response to loading frequency may still hold. Importantly, there appears to be a major distinction between the living cell behavior and the continuum model prediction: although the total displacement area was much lower at 30 Hz than at 0.3 Hz, there were obvious displacements at remote sites ( $>20 \mu\text{m}$  from the loading site) at 30 Hz loading frequency (Fig. 5), suggesting that the long distance force propagation behavior was still present even at this relatively high loading frequency, consistent with our experimental results in previous studies (7-9), and consistent with our recent model predictions (23) that the prestress in the actin bundles is the key determinant of how far a force can propagate.

At this time we do not know the underlying mechanism for the biphasic behavior on loading frequency. We speculate that, however, at loading frequencies  $>5 \text{ Hz}$ , the dissipative/frictional nature of the CSK lattice and its crosslinkers might hinder lateral propagation of the stresses from the actin bundle to the rest of the CSK such that the microtubule filaments that are in the vicinity of (but not very close to) the actin bundle are not deformed/displaced. Therefore, the total displacement area is decreased. However, since the contractile prestress in the actin bundles does not change much, the stress is still able to be propagated to long distances along the actin bundle to displace/deform those microtubules that are very close to the bundle. Since microtubules near the focal adhesions may not depend on actin bundles to transmit stresses, we suggest that this is why peak mitochondria displacements very close to the magnetic bead do not decrease very much with loading frequency.

At the low loading frequency of 0.03 Hz, each loading cycle is  $\sim 30 \text{ sec}$ . There are ten fluorescent images per

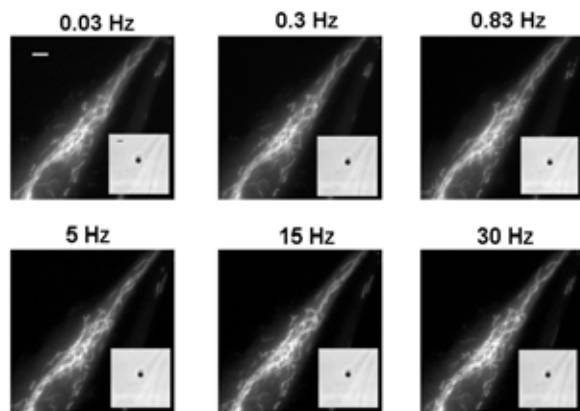


**Figure 9** : The fluorescent images and the bright field images (inserts) of a representative cell when loading frequency varies. There is no apparent bleaching or obvious changes in cell shape or bead position at different loading frequencies. Scale bar is  $5 \mu\text{m}$  for both the fluorescent image and the bright field image.

cycle. Thus the duration between an image and its subsequent image (for image cross-correlation analysis) is  $\sim 3$  sec, long enough for significant CSK remodeling to occur. When the threshold of 3 of the signal-to-noise ratio was used to filter out the noise, it is likely that some signals were also filtered out together with the remodeling-associated displacements. Therefore, it is possible that the measured displacement area at 0.03 Hz is an underestimate of the true value. Nevertheless, the conclusion that the total mitochondria displacement area (or the extent of stress propagation) varies with loading frequency in a biphasic manner may not change. It is interesting to note that the loading frequencies (0.3-0.8 Hz) that induce the maximum displacement area fall within the physiologic range (0.2-1.0 Hz) that these cells experience *in vivo*.

When a mechanical stress is applied to a living cell, it will induce biochemical and biological changes in the cell (26, 27). The challenge is to separate the direct mechanical displacement/deformation from stress-induced structural changes such as CSK remodeling. Our results suggest that at loading frequencies higher than 0.3 Hz, the synchronous detection approach is relatively robust and the effect of CSK remodeling on stress-induced displacement measurements is very small (Fig. 8). When the local load was applied for more than 10 min, how-

ever, we observed some subtle changes in the displacement patterns (not shown). These subtle changes could be due to spontaneous bead movements as a result of focal adhesion dynamics, CSK dynamics, membrane ruffling, stress-induced CSK remodeling, or a combination of all these. Future work is needed to determine which of these plays what role at what time.

Our results are consistent with a recent study that visualizes long distance propagation of Src activation in living cells in response to a localized load (26). It will be interesting to determine to what degree the location and the extent of Src activation depend on the cytoskeletal prestress or by loading frequency. It also remains to be seen if other cytoplasmic molecules and nuclear molecules can be directly activated by a localized load of physiologic magnitudes applied at the cell surface.

Our current study suggests that one cannot predict the stress propagation patterns of the cell simply from the rheological properties of a living cell. Unlike the stiffness of the cell that increases weakly with loading frequency, the extent of stress propagation exhibit a biphasic behavior (first increase and then decrease) with loading frequency. Regional connectivity differences of the CSK and local prestress variability in the CSK may exert significant influences on the stress distribution in the cytoplasm in response to a localized load on the cell surface. The stress propagation patterns could determine the specific sites of intracellular biochemical activities and the overall biological response from the cell.

**Acknowledgement:** We thank Dr. D. Stamenovic for critically reviewing this manuscript. This work was supported by NIH R01 GM072744.

#### **Appendix A: Sub-micrometer bead loading also leads to long-distance force propagation**

Previously, we showed evidence of long distance force transmission in the CSK in response to a localized load (7). One question is, however, whether this “action at a distance” is the artifact of large focal adhesion at the cell apical surface induced by the  $4.5\text{-}\mu\text{m}$  bead. To address this question, we coated  $0.8\text{-}\mu\text{m}$  ferromagnetic beads with RGD-peptides and added the beads to the cell apical surface for  $\sim 5$  min. A single bead on a cell infected with adenovirus YFP-mitochondria was located via

the microscope (Fig. 7A, 7B). After magnetization in the horizontal direction, a 0.83-Hz sinusoidal torque (25 gauss; specific torque = 2.5 Pa) was applied via the bead in the vertical direction. The induced displacement map showed distinct, concentrated displacements at sites  $\sim 5\text{--}7\ \mu\text{m}$  away from the bead (Fig. 7C). Assuming that the bead was 50% embedded, we estimated that the area of integrin clustering induced by this sub-micrometer bead is  $\sim 1\ \mu\text{m}^2$ . This result showed that a localized load applied via clustered integrin receptors of  $1\ \mu\text{m}^2$  could also be propagated to long distances along the CSK in the cytoplasm. From the bead displacement we estimated that the cell shear modulus was  $\sim 423\ \text{Pa}$ . Assuming that the average cell shear modulus was  $423\ \text{Pa}$ , we computed an intracellular traction map (Fig. 7D) at this focal plane ( $\sim 2\ \mu\text{m}$  above the cell base) in response to the sub-micrometer bead loading.

When mechanical properties of a material or a cell are probed, a key issue is: what is the probe size relative to the length scale of materials to be probed. In a living adherent cell, the persistent length of actin filaments is  $\sim 15\ \mu\text{m}$ , of intermediate filaments  $\sim 1\ \mu\text{m}$ , of microtubule filaments  $\sim 6\ \text{mm}$ . Thus the probe size should be  $\sim 1\text{--}5\ \mu\text{m}$  if one is interested in probing mechanical properties of the CSK lattice. We have demonstrated in this study that a submicrometer bead also induces an “action at a distance” phenomenon, consistent with the previous findings using a  $4\text{-}\mu\text{m}$  bead. It is possible, however, if the probe size is  $\ll 100\ \text{nm}$ , much smaller than the length scale of the CSK network, only very local cytosolic properties or single filament properties (if the bead is attached to the filament) rather than the CSK network properties can be probed.

## References

1. Wang, N., Butler, J.P. & Ingber, D.E. (1993) *Science* **260**, 1124-1127.
2. Choquet, D., Felsenfeld, D. P. & Sheetz, M.P. (1997) *Cell* **88**, 39-48.
3. Balaban, N.Q., Schwarz, U. S., Riveline, D., Goiberg, P., Tzur, G., Sabanay, I., Mahalu, D., Safran, S., Bershadsky, A., Addadi, L., et al. (2001) *Nat. Cell Biol.* **3**, 466-472.
4. Wang, N., Naruse, K., Stamenovic, D., Fredberg, J.J., Mijailovich, S.M., Tolic-Norrelykke, I.M., Polte, T., Mannix, R. & Ingber, D.E. (2001) *Proc. Natl. Acad. Sci U.S.A.* **98**, 7765-7770.
5. Jiang, G., Giannone, G., Critchley, D.R., Fukumoto, E. & Sheetz, M.P. (2003) *Nature* **424**, 334-7.
6. Wang, N. (1998) *Hypertension* **32**, 162-165.
7. Hu, S., Chen, J., Fabry, B., Numaguchi, Y., Gouldstone, A., Ingber, D.E., Fredberg, J.J., Butler, J.P. & Wang, N. (2003) *Am. J. Physiol. Cell Physiol.* **285**, C1082-C1090.
8. Hu, S., Eberhard, L., Chen, J., Love, J.C., Butler, J.P., Fredberg, J.J., Whitesides, G.M. & Wang, N. (2004) *Am. J. Physiol. Cell Physiol.* **287**, C1184-C1191.
9. Hu, S., Chen, J., Butler, J.P. & Wang, N. (2005) *Biochem. Biophys. Res. Commu.* **329**, 423-428.
10. Mijailovich, S.M., Kojic, M., Zivkovic, M., Fabry, B. & Fredberg, J.J. (2002) *J. Appl. Physiol.* **93**, 1429-1436.
11. Wang, N., Tolic-Norrelykke, I.M., Chen, J., Mijailovich, S.M., Butler, J.P., Fredberg, J.J. & Stamenovic, D. (2002) *Am. J. Physiol. Cell Physiol.* **282**, C606-C616.
12. Fabry, B., Maksym, G.M., Butler, J.P., Glogauer, M., Navajas, D. & Fredberg, J.J. (2001) *Phys. Rev. Lett.* **87**, 1481021-4.
13. Stamenovic, D., Mijailovich, S.M., Tolic-Norrelykke, I.M., Chen, J. & Wang, N. (2002) *Am. J. Physiol. Cell Physiol.* **282**, C617-C624.
14. Tanaka, Y., Kanai, Y., Okada, Y., Nonaka, S., Takeda Harada A.S. & Hirokawa, N. (1998) *Cell* **26**, 1147-58.
15. Dull, R.O., Tarbell, J.M. & Davies, P.F. (1992) *J. Vasc. Res.* **29**, 410-419.
16. Tschumperlin, D.J., Dai, G., Maly, I., Kikuchi, T., Laiho, L.H., McVittie, A.K., Haley, K.J., Lilly, C.M., So, P.T.C., Lauffenburger, D.A., et al. (2004) *Nature* **429**, 83-86.
17. Fung, Y.C. & Liu, S. Q. (1993) *ASME J. Biomech. Eng.* **115**, 1-12.

18. Gudi, S., Nolan, J.P. & Frangos, J.A. (1998) *Proc. Natl. Acad. Sci. USA* **95**, 2515-2519.
19. Davies, P. F. (1995) *Physiol. Rev.* **75**, 519-560.
20. Janmey, P.A. (1998). *Physiol. Rev.* **78**, 763-781.
21. Shyy, J.Y. & Chien, S. (2002) *Circ Res.* **91**, 769-75.
22. Ingber, D.E. (2006) *FASEB J.* **20**, 811-27.
23. Wang, N. & Suo, Z. (2005) *Biochem. Biophys. Res. Commu.* **328**, 1133-8.
24. Deguchi, S., Ohashi, T. & Sato, M. (2005) *J. Biomech.* Oct 6; [Epub ahead of print].
25. Stamenovic, D., Suki, B., Fabry, B., Wang, N. & Fredberg, J.J. (2004) *J. Appl. Physiol.* **96**, 1600-5.
26. Wang, Y., Botvinick, E.L., Zhao, Y., Borns, M.W., Usami, S., Tsien, R.Y. & Chien, S. (2005) *Nature* **434**, 1040-5.
27. Matthews, B.D., Overby, D.R., Mannix, R. & Ingber, D.E. (2006) *J Cell Sci.* **119**, 508-18.